Structural Control of Kinetics for Macrocycle Threading by Fluorescent Squaraine Dye in Water

César F. A. Gómez-Durán,[ID] Wenqi Liu, María de Lourdes Betancourt-Mendiola, and Bradley D. Smith*[ID]

Department of Chemistry and Biochemistry, University of Notre Dame, 236 Nieuwland Science Hall, South Bend, Indiana 46556, United States

S *Supporting Information*

ABSTRACT: While the general concept of steric speed bumps has been demonstrated in rotaxane shuttles and macrocycle threading systems, the sensitivity of speed bump effects has not been evaluated as a function of structural geometry. Values of K_a and k_{on} for macrocycle threading in water are reported for a series of homologous squaraine dyes with different substituents (speed bumps) on the flanking chains and two macrocycles with different cavity sizes. Sensitivity to a steric speed bump effect was found to depend on (a) structural location, being lowest when the speed bump was near the end of a flanking chain, and (b) macrocycle cavity size, which was enhanced when the cavity was constricted. This new insight is broadly applicable to many types of molecular threading systems.

Sensitivity to Speed Bump Effect Depends on:
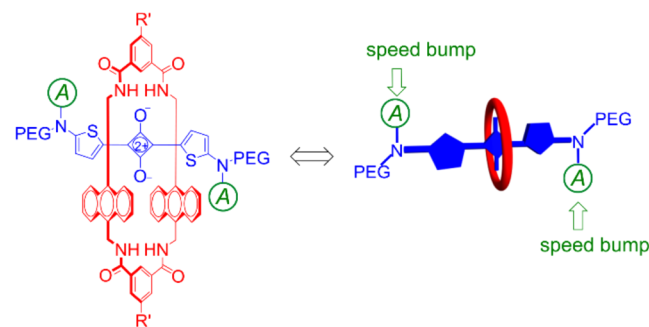Structural Location of Speed Bump   Macrocycle Cavity Size

INTRODUCTION

Pseudorotaxanes are the inclusion complexes formed when a macrocycle is threaded by a long axle molecule. Because of their unique dynamic and supramolecular properties, pseudorotaxanes are under active investigation for a wide range of applications in nanotechnology, materials science, and biomedicine.[1,2] Structural control of the thermodynamics and kinetics for macrocycle threading is a desirable capability since it greatly facilitates the process of optimizing molecular performance. A recent computational study by Sevick and Williams concluded that threading is a very rare complexation event with a high entropic penalty and that geometrical features, such as length and thickness of the axle, and internal diameter of the macrocycle, greatly affect the rate and extent of threading.[3] The challenge for supramolecular chemists is to design macrocycle/axle pairs with complementary shapes that provide enthalpic interactions between the interlocked components to overcome the inherent entropic barrier for threading. In the simplest case of a [2] rotaxane, the axle structure is usually composed of an internal docking station with appended chains. To reach the docking station, the macrocycle must slide on to the end of one of the flanking chains and translocate over any intervening steric elements within the chain. This mechanistic picture suggests that the rate of threading can be structurally controlled by incorporating steric speed bumps into the chains. To date, most studies of steric speed bumps have examined rotaxane systems that exhibit shuttling behavior,[4−13] with less attention on macrocycle threading systems.[14−20] Furthermore, the sensitivity of speed bump effects in macrocycle threading systems has not been explored as a function of geometric variables such as

location of the speed bump on the axle structure or relative size of the macrocycle cavity.

In recent years, we have developed a macrocycle threading system called Synthavidin (Synthetic Avidin) that is endowed with favorable optical properties that enable thermodynamic and kinetic measurements.[20] In short, a tetralactam macrocycle **M** with anthracene sidewalls is threaded by a deep-red fluorescent squaraine dye **S** with appended polyethylene glycol (PEG) chains to give the threaded complex **M⊃S** (Scheme 1). In water, macrocycle threading is very fast, and the association constant (K_a) is around 10^9 M^{-1}.[21] Systematic structural studies have measured the rate constant (k_{on}) for macrocycle threading

Scheme 1. Rate of Macrocycle Threading by Squaraine Dye To Give the Complex M⊃S Is Controlled by the Size of the Speed Bump Groups A
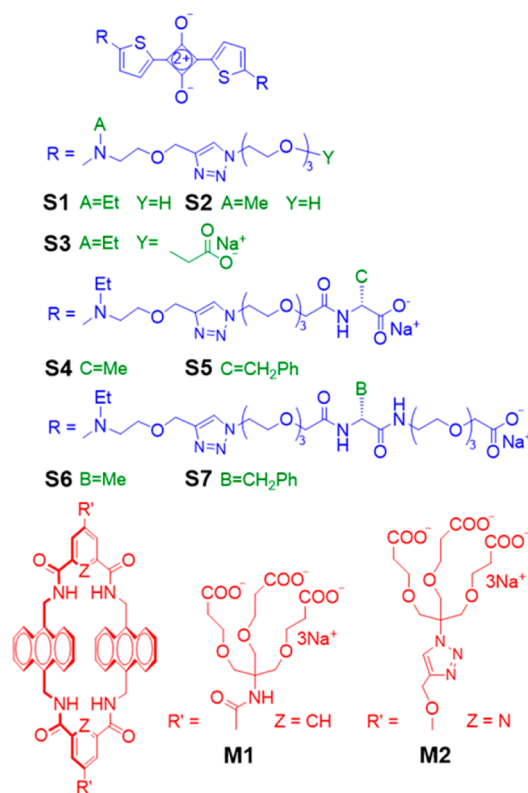
by homologous squaraine dyes that are flanked by amino groups bearing different *N*-substituents.[22] The identity of the *N*-substituents was found to have little influence on K_a, but in some cases there was a large effect on the threading kinetics. More specifically, k_{on} hardly changed when the length of an appended PEG chain was increased by many hundreds of atoms, but k_{on} was greatly affected by small steric changes to the second substituent (*A*) attached to the nitrogen. In other words, the *A* group was acting as a steric speed bump that controlled the rate of macrocycle threading. Structural control of the threading kinetics has allowed us to optimize the Synthavidin self-assembly properties for different types of applications. In one set of cases, we have used squaraine dyes with *A* = *N*-propyl to preassemble threaded fluorescent probes with high mechanical stability for long-term molecular imaging of living subjects.[23,24] A different Synthavidin project used squaraine dyes with *A* = *N*-methyl to ensure rapid capture of the dye after it was liberated by an enzyme-catalyzed cleavage process.[25]

In order to optimize supramolecular performance, we have to learn how much the kinetics for Synthavidin threading depends on changes in molecular structure, and here we address two questions that are fundamental to any macrocycle threading system. Does the magnitude of a steric speed bump effect change with spatial location on the squaraine axle? Does sensitivity to a speed bump effect increase when the macrocycle cavity is constricted? To answer these questions, we synthesized the squaraine dyes and macrocycles shown in Scheme 2 and measured K_a and k_{on} for macrocycle threading in water.

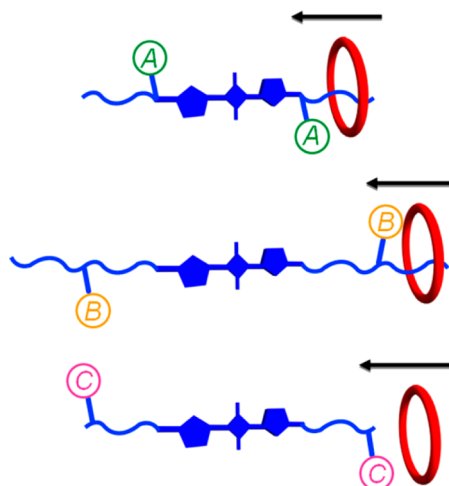**Scheme 2. Squaraine Dyes and Macrocycles Used in This Study**

RESULTS AND DISCUSSION

Does Sensitivity to a Steric Speed Bump Effect Change with Spatial Location on the Squaraine Axle? The speed bump effect was determined at three squaraine locations, labeled in Scheme 3 as *A*, *B*, and *C*. This was achieved
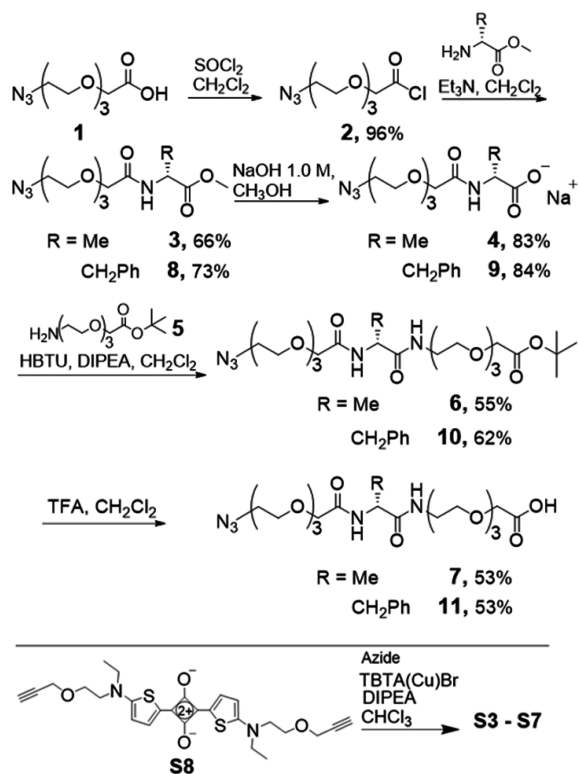
Scheme 3. Schematic Picture of the Three Speed Bump Locations, *A*, *B*, and *C*

by preparing the new squaraine dyes **S3**–**S7** using the sequence of conjugation reactions shown in Scheme 4. Since each dye had the same squaraine core there was little difference in the deep-red absorption and emission properties. Values of K_a and k_{on} for threading of macrocycle **M1** by each squaraine dye in water were measured using the same titration and stopped-flow methods employed in previous studies.[22,26] In each case, macrocycle threading was indicated by a diagnostic ~30 nm red-shift in squaraine fluorescence maxima (Table 1). In addition, the threaded complex (**M⊃S**) exhibited efficient internal fluorescence energy transfer; that is, when the anthracene sidewalls of the surrounding macrocycle (**M**) were excited with UV light there was greatly enhanced deep-red fluorescence emission from the encapsulated squaraine (**S**). Entries 1 and 2 in Table 2 provide a point of calibration for the previously observed steric speed bump effect at location *A*.[22] These studies used uncharged squaraine dyes **S1** and **S2**. When the *A* substituent was an *N*-ethyl group (**S1**, entry 1), k_{on} was measured to be $(1.2 \pm 0.1) \times 10^7$ M^{-1} s^{-1}. Decreasing the substituent size by one carbon atom to *N*-methyl (**S2**, entry 2) increased k_{on} by a factor of 100, indicating high sensitivity to the size of the speed bump at location *A*.

A common structural feature of the new squaraines used to measure the steric speed bump effect at locations *B* and *C* is an anionic carboxylate at the end of each flanking chain. This terminal carboxylate was included in the molecular designs to ensure that the dyes maintained high solubility in water and did not self-aggregate. Since **M1** has a −6 charge, we suspected that the terminal carboxylate group would induce an electrostatic effect on the threading process,[27] and this was measured by comparing K_a and k_{on} for neutral **S1** with a terminal hydroxyl (entry 1) against its isosteric analogue **S3** (entry 3) with a terminal carboxylate. The values of K_a for each system were within a factor 6, a relatively small difference that was expected since the terminal carboxylate in **S3** is ~20 atoms away from the binding interface of the **M1⊃S3** complex. But k_{on} for

Scheme 4. Synthesis of Squaraine Dyes

Entry	Azide	Product	Yield
1	1	S3	33%
2	4	S4	32%
3	9	S5	22%
4	7	S6	43%
5	11	S7	32%

Table 1. Absorption and Emission Maxima Wavelengths[a]

compd	λ_{abs} (nm)	λ_{em} (nm)
S3	660	674
M1⊃S3	676	706
S4	645	665
M1⊃S4	665	711
S5	663	676
M1⊃S5	676	708
S6	662	676
M1⊃S6	676	706

[a]In H_2O (5 μM).

threading of M1 by anionic S3 was about 600 times lower than neutral S1. The slower threading by S3 is presumably due to the increase in electrostatic repulsion that accrues when the anionic terminal carboxylate group approaches the multianionic M1. Since the flanking chains in squaraines S4−S7 all have a terminal carboxylate, we assume a similar electrostatic effect is operating in each case and thus any relative differences in K_a and k_{on} can be attributed to a steric speed bump effect at locations B or C.

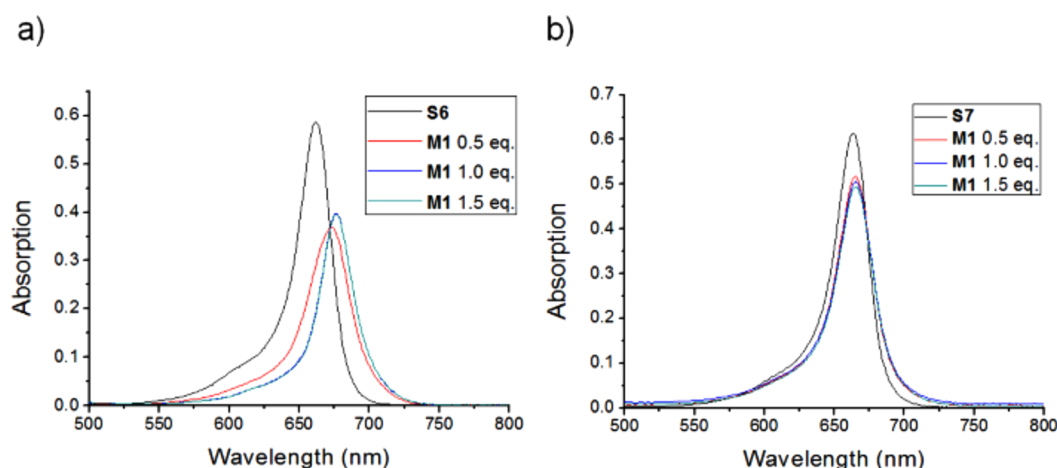The speed bump effect at terminal position C was assessed by comparing K_a and k_{on} for the two squaraines S4 and S5

Table 2. Association Constants (K_a) and Threading Rates (k_{on}) for Association of Squaraine and Macrocycle at 20 °C

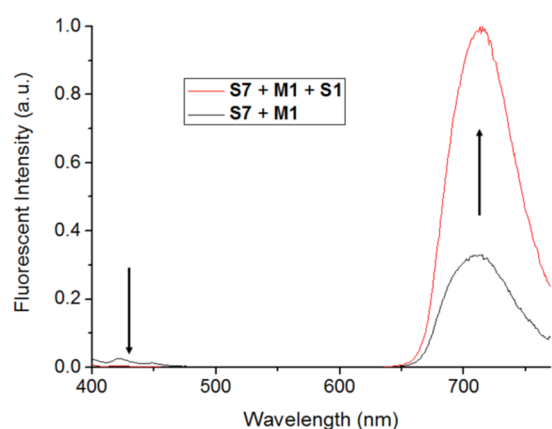| entry	squaraine	macrocycle	K_a (M^{-1})	k_{on} (M^{-1} s^{-1})
1[a]	S1	M1	$(6.0 \pm 1.2) \times 10^8$	$(1.2 \pm 0.1) \times 10^7$
2[a]	S2	M1	$(1.2 \pm 0.5) \times 10^9$	$(1.1 \pm 0.1) \times 10^9$
3	S3	M1	$(1.0 \pm 0.6) \times 10^8$	$(1.9 \pm 0.2) \times 10^4$
4	S4	M1	$(5.8 \pm 0.1) \times 10^7$	$(2.0 \pm 0.1) \times 10^4$
5	S5	M1	$(6.5 \pm 0.2) \times 10^8$	$(2.0 \pm 0.1) \times 10^4$
6	S6	M1	$(3.5 \pm 0.1) \times 10^8$	$(6.6 \pm 0.2) \times 10^4$
7	S7	M1	no threading	
8	S1	M2	$(2.1 \pm 0.2) \times 10^7$	$(2.6 \pm 1.2) \times 10^3$
9	S2	M2	$(1.5 \pm 0.6) \times 10^9$	$(5.4 \pm 0.8) \times 10^6$

[a]Data for this entry taken from ref 22.

which have the same squaraine core but different groups near the very end of the flanking chains. The N-acylalanine group in S4 is much smaller than the N-acylphenylalanine group in S5, and a comparison of entries 4 and 5 in Table 2 shows little variation in K_a as expected, but surprisingly, there was also no difference in k_{on}. This means that the rate of macrocycle threading is quite insensitive to the size of a speed bump group at squaraine location C very near the end of a flanking chain.[28] The speed bump effect at midpoint position B was assessed by comparing the measured values of K_a and k_{on} for squaraines S6 and S7 whose structures have the same squaraine core and terminal carboxylates but differ by having alanine or phenyl-alanine units inserted near the midpoint of the flanking chains. A comparison of entries 6 and 7 in Table 2 shows that the smaller alanine unit in S6 did not hinder threading of M1, but the effect of the larger phenylalanine unit in the case of S7 was profound in that it completely blocked macrocycle threading. This conclusion is based on the following experimental observations. Unlike the threading process that formed M1⊃S6 with a significant squaraine red-shift effect (Figure 1a), there was very little change in the squaraine absorption band when M1 and S7 were mixed in equal molar amounts (Figure 1b). In addition, an equal molar sample of M1 and S6 exhibited efficient energy transfer from excited M1 to S6, whereas an equal molar sample of M1 and S7 produced very weak energy transfer (Figure 2). Furthermore, a competitive energy transfer experiment showed that the presence of S7 did not inhibit the threading of M1 by a subsequent addition of S1 (Figure 2). It was not possible to monitor the interaction of M1 and S7 by ^{1}H NMR because S7 self-aggregates at millimolar concentrations in water and the NMR signals are very broad. However, independent verification that M1 is not threaded by S7 was gained by conducting an insightful TLC experiment. We have previously shown that the presence of M1 completely prevents elution of S1 up a TLC plate due to formation of a very polar M1⊃S1 complex.[21] Using the same TLC conditions, we find that the presence of M1 does not alter the R_f of S7, indicating that a threaded complex is not formed (Figure S61).

Taken together, the results in Table 2 show that the presence of substituents on the chains appended to the squaraine dyes can lower k_{on} for macrocycle threading but sensitivity to the substituent's steric size (speed bump effect) depends on the location. There is high steric sensitivity at locations A and B, but very low steric sensitivity at location C. *It is worth emphasizing that this conclusion focuses on the sensitivity to a speed bump effect at different locations. It is not valid to compare absolute values of k_{on} for speed bumps at two different locations.* An explanation for the difference in sensitivities is provided by

Figure 1. Absorption spectra for 5 μM samples of: (a) **S6** or (b) **S7** before and after addition of aliquots of **M1** in H_2O at 20 °C.
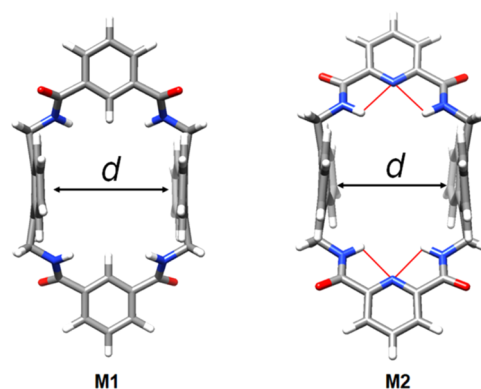

Figure 2. Change in fluorescence spectra (ex: 390 nm) caused by addition of **S1** (5 μM) to a mixture of **S7** (5 μM) and **M1** (5 μM) in H_2O at 20 °C. The decrease in anthracene emission at 420 nm and concomitant increase in squaraine emission at 715 nm indicates formation of **M1⊃S1** with enhanced fluorescence energy transfer from excited **M1** to **S1**.

inspecting Scheme 3. At locations *A* and *B* there is high sensitivity because the macrocycle cavity is already partially occupied by a segment of the oxyethylene chain which makes it harder for the macrocycle to translocate over the speed bump. In contrast, the speed bump group at location *C* has the option of passing through the macrocycle before the oxyethylene chain which makes it easier to avoid steric congestion. Knowing the sensitivity to speed bump sterics at each location along the squaraine structure will greatly help our future efforts to design cleavable squaraine systems for in situ capture applications such as turn-on fluorescent enzyme assays.[25] These applications require a squaraine structure with blocking groups that ensure no macrocycle threading until the groups are cleaved. At position *C* a blocking group would have to be relatively large, but at positions *A* and *B* a blocking group could be substantially smaller.

Does Sensitivity to Speed Bump Effect Increase when the Macrocycle Cavity Is Constricted? In principle, an alternative way to enhance the magnitude of a steric speed bump effect is to reduce the internal diameter of the macrocycle cavity. Previously, we and others have shown that a useful way to contract the cavity of a tetralactam macrocycle is to change the bridging units from 1,3-benzene dicarboxamide to 1,3-

pyridine dicarboxamide.[29−31] X-ray crystal structures show that the pyridine nitrogen atom forms hydrogen bonds with the two adjacent NH residues which reduces the angle between the two carboxamides and shortens the distance *d* between the two parallel aromatic sidewalls (Figure 3).[32] Furthermore, the
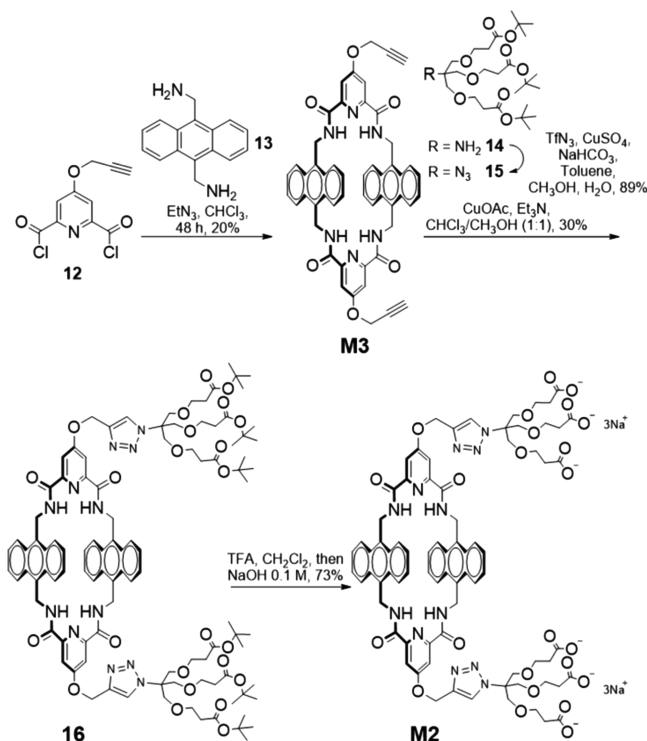

Figure 3. Calculated cavity sizes for macrocycles with 1,3-benzene dicarboxamide (left) and 1,3-pyridine dicarboxamide (right) bridging units with the red lines representing intramolecular hydrogen bonds. The cavity sizes were calculated using the PM7 method and match the trend seen with X-ray structures of squaraine rotaxanes where *d* values for analogues of **M1** (6.91−7.18 Å) are longer than *d* values for analogues of **M2** (6.61−6.78 Å).[32]

internal hydrogen bonding rigidifies the macrocycle and makes it harder for the cavity to transiently expand its size by adopting a conformation that directs an NH residue out of the cavity.[29]

To assess if macrocycle cavity contraction had any significant effect on the threading process, we prepared the new water-soluble macrocycle **M2**. The compound was made in rapid fashion by first preparing the appropriate bis-alkyne macrocycle **M3** and then conducting a copper-catalyzed azide/alkyne cycloaddition reaction to attach dendritic arms that provided useful water solubility after removal of the protecting groups (Scheme 5). As expected, squaraine threading of **M2** produced the diagnostic ∼30 nm red-shift in squaraine fluorescence maxima and large enhancement in squaraine fluorescence quantum yield (Table 3).

We measured K_a and k_{on} for threading of **M2** by uncharged squaraines **S1** and **S2** and compared the results to threading of **M1**. A schematic picture of this comparison is shown in
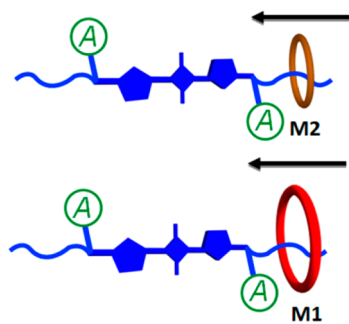
Scheme 5. Synthesis of M2

Table 3. Photophysical Data[a]

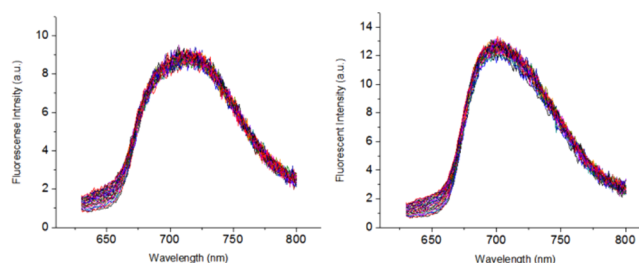| compd	λ_{abs} (nm)	λ_{ex} (nm)	λ_{em} (nm)	Φ_f
S1	660	668	678	0.04
S1⊃M2	673	660	699	0.23
S2	656	660	670	0.02
S2⊃M2	671	660	701	0.20

[a]In H_2O (5 μM).

Scheme 6. In the case of **S2** (A = N-methyl), k_{on} for threading of **M2** was slower by a factor of 200 (Table 2, compare entries

Scheme 6. Magnitude of the Steric Speed Bump Effect with M2 Is Increased because the Internal Diameter of the Macrocycle Cavity Is Reduced

2 and 9). With **S1** (A = N-ethyl) the difference was larger, and the k_{on} for threading of **M2** was slower by 5000 (compare entries 1 and 8). These results show that the constricted cavity for **M2** greatly slows the rate of macrocycle threading. The related question of whether the constricted cavity induces a greater sensitivity to changes in speed bump size is answered by comparing the change in free energies of activation ($\Delta G^{\ddagger}$) for threading by **S2** (A = N-methyl) and by **S1** (A = N-ethyl). With

M1, the difference in free energies of activation ($\Delta\Delta G^{\ddagger}$) is 2.7 kcal mol^{-1}, and for **M2**, $\Delta\Delta G^{\ddagger}$ is 4.6 kcal mol^{-1}. Thus, threading of the constricted **M2** is not only slower but $\Delta G^{\ddagger}$ is more sensitive to changes in speed bump sterics. One of the planned applications with these threaded complexes is biological imaging, and it is helpful if the preassembled complexes have high mechanical stability in biological fluids. As a preliminary test, we measured the stability of the preassembled complexes **M2 ⊂ S2** and **M2 ⊂ S1** in fetal bovine serum (FBS), and as shown in Figure 4 there was no fluorescence evidence for complex unthreading after 15 h.

Figure 4. Fluorescence spectra (ex: 620 nm) show no significant dissociation of (left) **M2⊃S2** and (right) **M2⊃S1** (5 μM) in FBS over 15 h (spectra acquired every 30 min).

◼ CONCLUSION

While speed bump effects have been reported for various threaded molecular systems,[14−19] this is the first systematic demonstration that sensitivity to the effect (a) depends on the structural location and decreases in the order of locations A ∼ B > C (Scheme 3) and (b) is enhanced when the macrocycle cavity size is constricted (Scheme 6). This new insight is relevant for many types of rotaxane shuttles and pseudorotaxane threading systems and will aid community efforts to optimize the kinetics for dynamic molecular devices such as sensors, actuators, capture agents, and processive catalysts.[1−19] It will especially help us to design next-generation Synthavidin pairs for in situ capture of enzyme reaction products and preassembly of fluorescent molecular probes.[23−25]

◼ EXPERIMENTAL SECTION

Synthesis. Compounds **S8**,[21] **1**,[33] **5**,[34] and **M1**[35] were synthesized using previously reported methods. The synthesis of squaraines **S1**[21] and **S2**[22] have been reported previously and were confirmed by NMR, UV/vis, and fluorescence spectroscopy. High-resolution mass spectrometry (HRMS) was performed using a TOF mass analyzer.

Acid Chloride Azide 2. Compound **1** (100 mg, 0.42 mmol) was dissolved in CH_2Cl_2 (2 mL). Thionyl chloride (102 mg, 0.87 mmol) was added to reaction mixture. The mixture was stirred overnight at room temperature. The solvent was removed to yield **2** as a brown viscous liquid (104 mg, 96% yield): ^{1}H NMR (500 MHz, CDCl$_3$) δ 4.48 (s, 2H), 3.80−3.73 (m, 2H), 3.68−3.57 (m, 8H), 3.41−3.33 (m, 2H); ^{13}C{^{1}H} NMR (125 MHz, CDCl$_3$) δ 172.0, 71.3, 70.7, 70.6, 70.5, 70.0, 50.6.

General Procedure for the Synthesis of Compounds 3 and 8. Compound **2** (1.19 mmol), Et$_3$N (1.42 mmol), and methyl ester derivative (1.42 mmol) were dissolved in CH_2Cl_2 (3 mL). The reaction mixture was stirred overnight at room temperature. The mixture was dried and dissolved in CHCl$_3$ and washed with H_2O. The organic layer was evaporated under vacuum to yield the desired derivative as a brown viscous liquid.

Data for compound 3: 270 mg, 73% yield; ^{1}H NMR (500 MHz, CDCl$_3$) δ 7.29 (d, J = 7 Hz, 1H), 4.59 (quin, J = 7 Hz, 1H), 3.98 (s,

2H), 3.74–3.57 (m, 13H), 3.36–3.34 (m, 2H), 1.39 (d, J = 7 Hz, 3H); ^{13}C{^{1}H} NMR (125 MHz, CDCl$_3$) δ 173.0, 169.5, 71.0, 70.6, 70.3, 70.2, 70.0, 52.3, 50.6, 47.3, 18.1; HRMS-ESI m/z calcd 341.1432 for [M + Na]$^+$ C$_{12}$H$_{22}$N$_4$O$_6$Na$^+$, found 341.1451.

Data for compound 8: 104 mg, 66% yield; ^{1}H NMR (500 MHz, CDCl$_3$) δ 7.25–7.03 (m, 5H), 4.88 (m, 1H), 3.96, 3.94 (ABq, J_{AB} = 6 Hz, 2H), 3.75–3.49 (m, 14H), 3.35 (s, 2H), 3.22, 3.12 (ABq, J = 6 Hz, 2H); ^{13}C{^{1}H} NMR (125 MHz, CDCl$_3$) δ 171.7, 169.6, 135.9, 129.2, 128.5, 127.0, 71.0, 70.6, 70.4, 70.3, 70.0, 52.6, 52.2, 50.6, 37.9; HRMS-ESI m/z calcd for 395.1925 [M + H]$^+$ C$_{18}$H$_{27}$N$_4$O$_6^+$, found 395.1923.

General Procedure for the Synthesis of Compounds 4 and 9. Compound 3 or 8 (0.22 mmol) was dissolved in MeOH (2 mL), and then a solution of NaOH (1 M, 5 mL) was added. After 12 h, the solvent was removed, and the residue was extracted by CHCl$_3$ and dried over MgSO$_4$ to give desired derivative as a viscous liquid.

Data for compound 4: 55 mg, 83% yield; ^{1}H NMR (500 MHz, CDCl$_3$) δ 7.47 (d, J = 7 Hz, 1H), 4.60 (quin, J = 7 Hz, 1H), 4.05 (s, 2H), 3.76–3.63 (m, 10H), 3.39 (t, J = 5 Hz, 2H), 1.47 (d, J = 7 Hz, 3H); ^{13}C{^{1}H} NMR (125 MHz, CDCl$_3$) δ 175.2, 170.7, 71.0, 70.5, 70.2, 70.0, 69.9, 50.6, 47.6, 17.8; HRMS-ESI m/z calcd for 327.1275 [M + Na]$^+$ C$_{11}$H$_{20}$N$_4$O$_6$Na$^+$, found 327.1285.

Data for compound 9: 71 mg, 84% yield; ^{1}H NMR (500 MHz, CDCl$_3$) δ 7.35 (d, J = 8 Hz, 1H), 7.22 (m, 5H), 4.86 (q, J_{AB} = 7 Hz, 1H), 3.96, 3.92 (ABq, J_{AB} = 12 Hz, 2H), 3.73–3.46 (m, 12H), 3.35–3.27 (m, 2H), 3.26, 3.04 (ABq, J_{AB} = 14 Hz, 2H); ^{13}C{^{1}H} NMR (125 MHz, CDCl$_3$) δ 173.4, 170.8, 135.9, 129.2, 128.4, 127.0, 70.8, 70.4, 70.1, 69.8, 52.6, 50.5, 37.3; HRMS-ESI m/z calcd for 403.1588 [M + Na]$^+$ C$_{17}$H$_{24}$N$_4$NaO$_6^+$, found 403.1615.

General Procedure for the Synthesis of 6 and 10. Compound 4 or 9 (0.10 mmol), HBTU (56 mg, 0.36 mmol), DIPEA (94 mg, 126 μL, 0.73 mmol), and compound 5 (25 mg, 0.24 mmol) were dissolved in CH$_2$Cl$_2$ (3 mL). The reaction mixture was stirred overnight at room temperature. The solvent was removed by vacuum in a rotary evaporator. H$_2$O (20 mL) was added to the residue, and the mixture was extracted with CHCl$_3$ (3 × 20 mL) and dried with anhydrous MgSO$_4$. The organic phases were evaporated by vacuum to give the desired product as a viscous liquid.

Data for compound 6: 32 mg, 55% yield; ^{1}H NMR (500 MHz, CDCl$_3$) δ 7.33 (d, J = 8 Hz, 1H), 6.77 (br s, 1H), 4.47 (quin, J = 7 Hz, 1H), 4.07–3.92 (m, 4H), 3.74–3.32 (m, 24H), 1.44 (s, 9H), 1.36 (d, J = 7 Hz, 3H); ^{13}C{^{1}H} NMR (101 MHz, CDCl$_3$) δ 172.0, 169.6, 169.6, 81.6, 71.0, 70.6, 70.6, 70.4, 70.4, 70.3, 70.2, 70.0, 69.6, 68.9, 50.6, 48.2, 39.3, 28.0, 18.3; HRMS-ESI m/z calcd for 550.3083 [M + H]$^+$ C$_{23}$H$_{43}$N$_5$O$_{10}^+$, found 550.3101.

Data for compound 10: 35 mg, 62% yield; ^{1}H NMR (500 MHz, CDCl$_3$) δ 7.41–7.28 (m, 1H), 7.27–7.09 (m, 5H), 6.55 (s, 1H), 4.68 (q, J_{AB} = 7 Hz, 1H), 4.00–3.83 (m, 4H), 3.72–3.40 (m, 20H), 3.37–3.25 (m, 4H), 3.12–2.96 (m, 2H), 1.49–1.38 (s, 9H); ^{13}C{^{1}H} NMR (126 MHz, CDCl$_3$) δ 170.4, 169.7, 169.6, 136.8, 129.3, 128.4, 126.8, 81.6, 70.9, 70.6, 70.6, 70.4, 70.4, 70.4, 70.3, 70.1, 70.0, 69.5, 68.9, 54.0, 50.6, 39.2, 38.3, 28.0; HRMS-ESI m/z calcd for 626.3396 [M + H]$^+$ C$_{29}$H$_{48}$N$_5$O$_{10}^+$, found 626.3385.

General Procedure for Compounds 7 and 11. Compound 6 or 10 (0.06 mmol) was dissolved in CH$_2$Cl$_2$ (2 mL), and TFA (1 mL) was added. The reaction mixture was stirred overnight at room temperature. The solvents were removed by vacuum in a rotary evaporator. NaOH (1 M) was added dropwise until pH 10, and the solution was washed with ethyl acetate. The aqueous phase was acidified by HCl (1 M) until pH 4, and the product was extracted with CHCl$_3$ (3 × 10 mL). The organic phase was dried over MgSO$_4$, and the solvent was removed by vacuum to give the desired product as a viscous liquid.

Data for compound 7: 23 mg, 53% yield; ^{1}H NMR (500 MHz, CDCl$_3$) δ 7.58 (d, J = 8 Hz, 1H), 7.17 (br s, 1H), 4.72–4.63 (m, 1H), 4.18 (s, 2H), 4.03 (s, 2H), 3.80–3.33 (m, 24H), 1.39 (d, J = 7 Hz, 3H); ^{13}C{^{1}H} NMR (101 MHz, CDCl$_3$) δ 172.3, 172.2, 170.5, 71.0, 71.0, 70.6, 70.4, 70.3, 70.3, 70.1, 70.0, 70.0, 69.6, 68.5, 50.6, 48.4, 39.3, 18.4; HRMS-ESI m/z calcd for 516.2276 [M + Na]$^+$ C$_{19}$H$_{35}$N$_5$NaO$_{10}^+$, found 516.2280.

Data for compound 11: 21 mg, 53% yield; ^{1}H NMR (500 MHz, CDCl$_3$) δ 7.62 (d, J = 9 Hz, 1H), 7.33–7.12 (m, 5H), 7.07 (s, 1H), 4.88 (q J_{AB} = 8 Hz, 1H), 4.32–4.11 (m, 2H), 4.06, 3.90 (ABq, J_{AB} = 8 Hz, 2H), 3.81–3.23 (m, 24H), 3.19–2.94 (m, 2H); ^{13}C{^{1}H} NMR (125 MHz, CDCl$_3$) δ 172.3, 170.5, 170.4, 136.6, 129.4, 128.4, 126.8, 71.0, 71.0, 70.6, 70.4, 70.3, 70.2, 70.1, 70.0, 70.0, 69.6, 68.3, 54.0, 50.6, 39.1, 38.7; HRMS-ESI m/z calcd for 570.2770 [M + H]$^+$ C$_{25}$H$_{39}$N$_5$O$_{10}^+$, found 570.2759.

General Procedure for the Synthesis of Symmetric Squaraines S3–S7. Squaraine S8 (28 mg, 0.07 mmol), azide 1 (38 mg, 0.16 mmol), TBTACu(I)Br (9 mg, 0.014 mmol, 20 mmol %), and DIPEA (122 mg, 167 μL, 0.40 mmol) were dissolved in CHCl$_3$ (3 mL) and stirred at room temperature for 12 h. Solvent was removed under reduced pressure, and the residue was purified by silica gel column chromatography to yield the desired squaraine dye as a blue sticky solid that did not exhibit a defined melting point.

Data for squaraine S3: 0–10% MeOH/CHCl$_3$ (18 mg, 33% yield); ^{1}H NMR (500 MHz, MeOD) δ 8.03 (s, 2H), 7.93–7.84 (br s, 2H), 6.60–6.46 (br s, 2H), 4.64 (s, 4H), 4.59 (t, J = 5 Hz, 4H), 3.97 (s, 4H), 3.89–3.85 (m, 4H), 3.82 (t, J = 5 Hz, 4H), 3.78 (d, J = 5 Hz, 4H), 3.71–3.55 (m, 20H), 1.32–1.27 (t, J = 7 Hz, 6H); ^{13}C{^{1}H} NMR (125 MHz, MeOD) δ 176.2, 170.6, 165.3, 144.1, 137.9, 124.4, 114.0, 110.1, 69.8, 69.6, 69.6, 69.3, 69.0, 67.0, 63.5, 53.2, 49.8, 49.6, 10.7; HRMS-ESI m/z calcd for 962.3525 for [M + H]$^+$ C$_{42}$H$_{58}$N$_8$O$_{14}$S$_2^+$, found 962.3526; UV–vis (H$_2$O) λ_{abs} 660 nm; fluorescence (H$_2$O) λ_{ex} 664 nm, λ_{em} 674 nm.

Data for squaraine S4: 0–20% MeOH/CHCl$_3$ (15 mg, 32% yield); ^{1}H NMR (500 MHz, MeOD) δ 7.99 (br s, 2H), 7.56 (br s, 2H), 6.26 (br s, 2H), 4.63–4.57 (m, 8H), 3.89 (m, 2H), 3.87–3.78 (m, 8H), 3.72 (br s, 4H), 3.69–3.42 (m, 30H), 1.39–1.29 (m, 2H), 1.20–1.04 (s, 6H); ^{13}C NMR, small quantity of material prevented ^{13}C analysis; HRMS-ESI m/z calcd for 1127.4148 [M + Na]$^+$ C$_{48}$H$_{68}$N$_{10}$O$_{16}$NaS$_2^+$, found 1127.4149; UV–vis (H$_2$O) λ_{abs} 645 nm; fluorescence (H$_2$O) λ_{ex} 655 nm, λ_{em} 665 nm.

Data for squaraine S5: 0–20% MeOH/CHCl$_3$ (16 mg, 22% yield); ^{1}H NMR (500 MHz, MeOD/CDCl$_3$) δ 8.00 (s, 2H), 7.87 (s, 2H), 7.28–7.06 (m, 10H), 6.53 (s, 2H), 4.61 (s, 4H), 4.55 (s, 4H), 4.00–3.67 (m, 18 H), 3.64–3.40 (m, 24H), 3.22, 3.07 (ABq, J_{AB} = 7 Hz, 4H), 1.27 (t, J = 7 Hz, 3H). ^{13}C NMR, small quantity of material prevented ^{13}C analysis; MS-ESI calcd for 1257.4966 [M + H]$^+$ C$_{60}$H$_{77}$N$_{10}$O$_{16}$S$_2^+$, found 1257.4949; UV–vis (H$_2$O) λ_{abs} 663 nm; fluorescence (H$_2$O) λ_{ex} 666 nm, λ_{em} 676 nm.

Data for squaraine S6: 0–20% MeOH/CHCl$_3$ (21 mg, 43% yield); ^{1}H NMR (500 MHz, CDCl$_3$) δ 7.95 (br s, 2H), 7.76 (s, 2H), 7.56 (br s, 2H), 7.38 (br s, 2H), 4.66 (s, 4H), 4.55 (m, 4H), 4.18 (s, 4H), 4.03 (s, 4H), 3.91–3.35 (m, 60H), 1.47–1.34 (d, J = 5 Hz, 6H), 1.31–1.20 (t, J = 6 Hz, 6H); ^{13}C NMR, small quantity of material prevented ^{13}C analysis; HRMS-ESI m/z calcd for 1505.6151 ([M + Na]$^+$ C$_{64}$H$_{98}$N$_{12}$NaO$_{24}$S$_2^+$, found 1505.6107); UV–vis (H$_2$O) λ_{abs} 662 nm; fluorescence (H$_2$O) λ_{ex} 666 nm, λ_{em} 676 nm.

Data for squaraine S7: 0–20% MeOH/CHCl$_3$ (16 mg, 32% yield); ^{1}H NMR (500 MHz, CDCl$_3$) δ 7.91 (br s, 2H), 7.71 (s, 2H), 7.54 (d, J = 9 Hz, 2H), 7.25–7.11 (m, 10H), 6.25 (br s, 2H), 4.87 (m, 2H), 4.61 (s, 4H), 4.53 (t, J = 5 Hz, 4H), 4.15 (s, 4H), 4.03–3.26 (m, 60H), 3.04, 3.00 (ABq, J_{AB} = 7 Hz, 4H), 1.25 (t, J = 7 Hz, 6H); ^{13}C NMR, small quantity of material prevented ^{13}C analysis; HRMS-ESI m/z calcd for 1633.6812 [M − H]$^-$ C$_{76}$H$_{105}$N$_{12}$O$_{24}$S$_2^-$, found 1633.6792; UV–vis (H$_2$O) λ_{abs} 663 nm; fluorescence (H$_2$O) λ_{ex} 667 nm, λ_{em} 677 nm.

Macrocycle M3. In a round-bottom flask under argon, anthracene diamine 13 (100 mg, 0.42 mmol) was dissolved in dried CHCl$_3$ (200 mL). Acid chloride 12 (109 mg, 0.42 mmol) was dissolved in dried CHCl$_3$ (50 mL) in a glass syringe and slowly added to the flask over a period of 24 h by syringe pump. When the addition was complete, the mixture was stirred for an additional 24 h. The solvent was removed, and the residue was purified by chromatography using 0–20% acetone/CHCl$_3$ to obtain product M3 as a yellow solid (71 mg, 20% yield): mp >260 °C; ^{1}H NMR (500 MHz, CDCl$_3$) δ 8.28 (d, J = 7 Hz, 8H), 8.07 (s, 4H), 7.62 (t, J = 6 Hz, 4H), 7.52 (d, J = 7, Hz, 8H), 5.60 (d, J = 6 Hz, 8H), 4.93 (d, J = 2 Hz, 4H), 2.67 (t, J = 2 Hz, 2H);

^{13}C{^{1}H} NMR (125 MHz, CDCl$_3$) δ 166.3, 162.7, 150.7, 130.2, 130.0, 129.2, 126.5, 126.3, 124.5, 124.2, 112.3, 76.6, 56.5, 56.2, 36.1; HRMS-ESI m/z calcd for 865.2745 [M + Na]$^+$ C$_{52}$H$_{38}$N$_6$NaO$_6$$^+$, found 865.2743.

Azide 15. The amine **14** (500 mg, 0.99 mmol), sodium bicarbonate (339 mg, 4.00 mmol), and copper sulfate (8 mg, 0.05 mmol) were dissolved in H$_2$O (5 mL). Trifluoromethanesufonyl azide (696 mg, 4.00 mmol) in MeOH (2 mL) was added. The mixture was stirred overnight. The solvents were removed, and the crude material was purified by column (0−10% MeOH/CHCl$_3$) to give the product **15** as viscous liquid (470 mg, 89% yield): ^{1}H NMR (500 MHz, CDCl$_3$) δ 3.70 (t, J = 6 Hz, 6H), 3.55 (s, 6H), 2.50 (t, J = 6 Hz, 6H), 1.47 (s, 27H); ^{13}C{^{1}H} NMR (125 MHz, CDCl$_3$) δ 170.6, 170.6, 80.5, 80.4, 70.7, 67.2, 65.5, 36.1, 36.1, 28.0, 28.0; HRMS-ESI m/z calcd for 554.3048 [M + Na]$^+$ C$_{25}$H$_{45}$N$_3$NaO$_9$$^+$, found 554.3063.

Compound 16. In a round-bottom flask under argon, compound **M3** (50 mg, 0.06 mmol) and the corresponding azide **15** (158 mg, 0.30 mmol) were dissolved in a mixture of CHCl$_3$ and MeOH (2 mL, 1:1 v/v). CuOAc (36 mg, 0.30 mmol) and Et$_3$N (30 mg, 0.30 mmol) were added, and the mixture was stirred for 48 h at room temperature. Saturated Na-EDTA and brine were added, and the mixture was extracted with CHCl$_3$. The organic phase was dried over MgSO$_4$. The solvent was then removed, and the crude material was purified by column (0−10% MeOH/CHCl$_3$) to give the product **16** as light yellow solid (33 mg, 30%): mp 178−180 °C; ^{1}H NMR (600 MHz, CDCl$_3$) δ 8.26 (dd, J = 7, 3 Hz, 8H), 8.07 (s, 4H), 8.05 (s, 2H), 7.61 (t, J = 5 Hz, 4H), 7.50 (dd, J = 7, 3 Hz, 8H), 5.57 (d, J = 5 Hz, 8H), 5.34 (s, 4H), 3.99 (s, 12H), 3.67 (t, J = 6 Hz, 12H), 2.45 (t, J = 6 Hz, 12H), 1.43 (s, 54H). ^{13}C{^{1}H} NMR (125 MHz, CDCl$_3$) δ 170.7, 167.2, 162.7, 150.6, 140.5, 130.3, 129.4, 126.6, 124.3, 112.1, 80.7, 70.7, 67.9, 67.4, 36.2, 29.8, 28.2; HRMS-ESI m/z calcd for 975.9514 [M + 2Na]$^{2+}$ C$_{102}$H$_{129}$N$_{12}$Na$_2$O$_{24}$$^{2+}$, found 975.9552.

Macrocycle M2. Protected macrocycle **16** (35 mg, 0.02 mmol) was dissolved in CH$_2$Cl$_2$ (10 mL) in an ice bath under Ar. TFA (2 mL) was added dropwise over 30 min. The resulting solution was stirred overnight, and solvent was removed. The residue was suspended in a mixture of MeOH/H$_2$O (4:6, 10 mL), and NaOH solution (0.1 M) was added dropwise until pH = 7. The solution was passed through a 0.45 μm syringe filter and condensed under high vacuum. The residue was further purified by C18 reversed-phase column chromatography using acetone/H$_2$O (0−8%). The corresponding fraction was collected and freeze-dried to obtain **M2** as a light yellow solid (22 mg, 73% yield): mp 216−218; ^{1}H NMR (500 MHz, MeOD) δ 8.42 (s, 2H), 8.27−8.19 (m, 8H), 8.03 (s, 4H), 7.49 (dd, J = 7, 3 Hz, 8H), 5.51 (s, 8H), 5.46 (s, 4H), 4.03 (s, 12H), 3.71 (t, J = 7 Hz, 12H), 2.41 (t, J = 7 Hz, 12H); ^{13}C{^{1}H} NMR (101 MHz, MeOD) δ 179.1, 167.1, 164.2, 150.5, 141.0, 130.1, 129.1, 126.3, 125.2, 124.2, 111.8, 70.1, 69.0, 68.4, 61.4, 37.9, 35.9; HRMS-ESI m/z calcd for 1591.5301 [M + Na]$^+$ C$_{78}$H$_{80}$N$_{12}$NaO$_{24}$$^+$, found 1591.5290.

ASSOCIATED CONTENT

Ⓢ Supporting Information

The Supporting Information is available free of charge on the ACS Publications website at DOI: 10.1021/acs.joc.7b01486.

> Spectra for all new compounds; photophysical properties, kinetic and thermodynamic data, computational data (PDF)

AUTHOR INFORMATION

Corresponding Author
*E-mail: smith.115@nd.edu.

ORCID Ⓘ
César F. A. Gómez-Durán: 0000-0002-7051-0722
Bradley D. Smith: 0000-0003-4120-3210

Notes
The authors declare no competing financial interest.

ACKNOWLEDGMENTS

REFERENCES

(1) Van Dongen, S. F. M.; Cantekin, S.; Elemans, J. A. A. W.; Rowan, A. E.; Nolte, R. J. M. *Chem. Soc. Rev.* **2014**, 43, 99−122.
(2) Xue, M.; Yang, Y.; Chi, X.; Yan, X.; Huang, F. *Chem. Rev.* **2015**, 115, 7398−7501.
(3) Sevick, E. M.; Williams, D. R. M. *Nano Lett.* **2016**, 16, 671−674.
(4) Dey, S. K.; Coskun, A.; Fahrenbach, A. C.; Barin, G.; Basuray, A. N.; Trabolsi, A.; Botros, Y. Y.; Stoddart, J. F. *Chem. Sci.* **2011**, 2, 1046−1053.
(5) Young, P. G.; Hirose, K.; Tobe, Y. *J. Am. Chem. Soc.* **2014**, 136, 7899−7906.
(6) Collin, J. P.; Durola, F.; Lux, J.; Sauvage, J. P. *New J. Chem.* **2010**, 34, 34−43.
(7) Jeppesen, J. O.; Becher, J.; Stoddart, J. F. *Org. Lett.* **2002**, 4, 557−560.
(8) Berná, J.; Alajarín, M.; Marín-Rodríguez, C.; Franco-Pujante, C. *Chem. Sci.* **2012**, 3, 2314−2320.
(9) Baggerman, J.; Haraszkiewicz, N.; Wiering, P. G.; Fioravanti, G.; Marcaccio, M.; Paolucci, F.; Kay, E. R.; Leigh, D. a.; Brouwer, A. M. *Chem. - Eur. J.* **2013**, 19, 5566−5577.
(10) Andersen, S. S.; Share, A. I.; Poulsen, B. L. C.; Kørner, M.; Duedal, T.; Benson, C. R.; Hansen, S. W.; Jeppesen, J. O.; Flood, A. H. *J. Am. Chem. Soc.* **2014**, 136, 6373−6384.
(11) Ashton, P. R.; Baxter, I.; Fyfe, M. C. T.; Raymo, F. M.; Spencer, N.; Stoddart, J. F.; White, A. J. P.; Williams, D. J. *J. Am. Chem. Soc.* **1998**, 120, 2297−2307.
(12) Bolla, M. A.; Tiburcio, J.; Loeb, S. J. *Tetrahedron* **2008**, 64, 8423−8427.
(13) Catalán, A. C.; Tiburcio, J. *Chem. Commun.* **2016**, 52, 9526−9529.
(14) Deutman, A. B. C.; Varghese, S.; Moalin, M.; Elemans, J. A. A. W.; Rowan, A. E.; Nolte, R. J. M. *Chem. - Eur. J.* **2015**, 21, 360−370.
(15) Deutman, A. B. C.; Monnereau, C.; Elemans, J. A. A. W.; Ercolani, G.; Nolte, R. J. M.; Rowan, A. E. *Science* **2008**, 322, 1668−1671.
(16) Arduini, A.; Bussolati, R.; Credi, A.; Secchi, A.; Silvi, S.; Semeraro, M.; Venturi, M. *J. Am. Chem. Soc.* **2013**, 135, 9924−9930.
(17) Cheng, C.; McGonigal, P. R.; Stoddart, J. F.; Astumian, R. D. *ACS Nano* **2015**, 9, 8672−8688.
(18) Yu, C.; Ma, L.; He, J.; Xiang, J.; Deng, X.; Wang, Y.; Chen, X.; Jiang, H. *J. Am. Chem. Soc.* **2016**, 138, 15849−15852.
(19) Senler, S.; Cheng, B.; Kaifer, A. E. *Org. Lett.* **2014**, 16, 5834−5837.
(20) Liu, W.; Samanta, S. K.; Smith, B. D.; Isaacs, L. *Chem. Soc. Rev.* **2017**, 46, 2391−2403.
(21) Peck, E. M.; Liu, W.; Spence, G. T.; Shaw, S. K.; Davis, A. P.; Destecroix, H.; Smith, B. D. *J. Am. Chem. Soc.* **2015**, 137, 8668−8671.
(22) Liu, W.; Peck, E. M.; Hendzel, K. D.; Smith, B. D. *Org. Lett.* **2015**, 17, 5268−5271.
(23) Peck, E. M.; Battles, P. M.; Rice, D. R.; Roland, F. M.; Norquest, K. A.; Smith, B. D. *Bioconjugate Chem.* **2016**, 27, 1400−1410.
(24) Roland, F. M.; Peck, E. M.; Rice, D. R.; Smith, B. D. *Bioconjugate Chem.* **2017**, 28, 1093−1101.
(25) Liu, W.; Gómez-Durán, C. F. A.; Smith, B. D. *J. Am. Chem. Soc.* **2017**, 139, 6390−6395.
(26) The thermodynamics and kinetics of association were determined from the changes in fluorescence or absorption. As shown in Figures S55−S60, each kinetic profile was fitted using first-order and second-order kinetic equations, and in each case, the second-order fit was equal or better than the first-order fit. Therefore, we assume a second-order threading model with translocation of the macrocycle over the speed bump as the rate-determining step.
(27) Carrasco-Ruiz, A.; Tiburcio, J. *Org. Lett.* **2015**, 17, 1858−1861.

(28) A reviewer makes the reasonable point that when a steric speed bump group is located near the very end of a flanking chain (such as location *C* in **S4** and **S5**) it is less clear what group is acting as the chain and what group is the speed bump. In this case it is simpler to consider both groups as a single unit (i.e., treat the combined groups as a stopper unit). From this perspective, the *N*-acylalanine stopper in **S4** is a much smaller than the *N*-acylphenylalanine stopper in **S5**; nonetheless, there is no difference in k_{on}.

(29) Murgu, I.; Baumes, J. M.; Eberhard, J.; Gassensmith, J. J.; Arunkumar, E.; Smith, B. D. *J. Org. Chem.* **2011**, *76*, 688−691.

(30) Affeld, A.; Hübner, G. M.; Seel, C.; Schalley, C. A. *Eur. J. Org. Chem.* **2001**, *2001*, 2877−2890.

(31) Johnston, A. G.; Leigh, D. A.; Nezhat, L.; Smart, J. P.; Deegan, M. D. *Angew. Chem., Int. Ed. Engl.* **1995**, *34*, 1212−1216.

(32) Baumes, J. M.; Murgu, I.; Oliver, A.; Smith, B. D. *Org. Lett.* **2010**, *12*, 4980−4983.

(33) Heller, K.; Ochtrop, P.; Albers, M. F.; Zauner, F. B.; Itzen, A.; Hedberg, C. *Angew. Chem., Int. Ed.* **2015**, *54*, 10327−10330.

(34) Chojnacki, J. E.; Liu, K.; Saathoff, J. M.; Zhang, S. *Bioorg. Med. Chem.* **2015**, *23*, 7324−7331.

(35) Ke, C.; Destecroix, H.; Crump, M. P.; Davis, A. P. *Nat. Chem.* **2012**, *4*, 718−723.